

1 Comparison of Image Registration Based Measures
2 of Regional Lung Ventilation from Dynamic Spiral CT
3 with Xe-CT
4

5 Kai Ding,^{1,*} Kunlin Cao,² Matthew K. Fuld,^{1,3}
6 Kaifang Du,¹ Gary E. Christensen,^{2,4} Eric A. Hoffman,^{1,3,**}
7 and Joseph M. Reinhardt^{1,**}

8 ¹Department of Biomedical Engineering,

9 ²Department of Electrical and Computer Engineering,

10 ³Department of Radiology,

11 ⁴Department of Radiation Oncology,

12 The University of Iowa, Iowa City, IA 52242

13 *Dr. Ding is currently with the Department of Radiation Oncology, University of Vir-
14 ginia, Charlottesville, VA 22908

15 **Drs. Reinhardt and Hoffman are founders and shareholder of VIDA Diagnostics, Inc.

1 **Correspondence:**

2 Joseph M. Reinhardt, PhD

3 Chair, Department of Biomedical Engineering

4 The University of Iowa

5 1402 SC

6 Iowa City, IA 52242

7 Tel. (319) 335-5634

8 FAX: (319) 335-5631

9 E-mail: joe-reinhardt@uiowa.edu

10

Abstract

Purpose: Regional lung volume change as a function of lung inflation serves as an index of parenchymal and airway status as well as an index of regional ventilation and can be used to detect pathologic changes over time. In this article, we propose a new regional measure of lung mechanics — the specific air volume change by corrected Jacobian. We compare this new measure, along with two existing registration-based measures of lung ventilation, to a regional ventilation measurement derived from xenon-CT (Xe-CT) imaging.

Methods: 4DCT and Xe-CT data sets from four adult sheep are used in this study. Nonlinear, 3D image registration is applied to register an image acquired near end inspiration to an image acquired near end expiration. Approximately 200 annotated anatomical points are used as landmarks to evaluate registration accuracy. Three different registration-based measures of regional lung mechanics are derived and compared: the specific air volume change calculated from the Jacobian (SAJ); the specific air volume change calculated by the corrected Jacobian (SACJ); and the specific air volume change by intensity change (SAI). We show that the commonly-used SAI measure can be derived from the direct SAJ measure by using the air-tissue mixture model and assuming there is no tissue volume change between the end inspiration and end expiration data sets. All three ventilation measures are evaluated by comparing to Xe-CT estimates of regional ventilation.

Results: After registration, the mean registration error is on the order of 1 mm. For cubical ROIs in cubes with size $20 \text{ mm} \times 20 \text{ mm} \times 20 \text{ mm}$, the SAJ and SACJ measures show significantly higher correlation (linear regression, average $r^2 = 0.75$ and $r^2 = 0.82$) with the Xe-CT based measure of specific ventilation (sV) than the SAI measure. For ROIs in slabs along the ventral-dorsal vertical direction with size of $150 \text{ mm} \times 8 \text{ mm} \times 40 \text{ mm}$, the SAJ, SACJ, and SAI all show high correlation (linear regression, average $r^2 = 0.88$, $r^2 = 0.92$ and $r^2 = 0.87$) with the Xe-CT based sV without significant differences when comparing between the three methods. We demonstrate a linear relationship between the difference of specific air volume change (DSA) and difference of tissue volume (DT) in all four animals (linear regression, average $r^2 = 0.86$).

Conclusion: Given a deformation field by an image registration algorithm, significant differences between the SAJ, SACJ, and SAI measures were found at a regional level compared to the Xe-CT sV in four sheep that were studied. The SACJ introduced here, provides better correlations with Xe-CT based sV than the SAJ and SAI measures, thus providing an improved surrogate for regional ventilation.

Keywords: image registration, ventilation, lung function, tissue function, pulmonary

1 Introduction

Regional ventilation is the term used to characterize the volume of fresh gas per unit time that enters or exits the lung at the acinar (gas exchange) level. Disruption of regional ventilation can reflect alterations to airways (physiological or pathological), alterations in parenchymal mechanics, changes to the muscles of respiration, body posture effects and inhaled gas properties. Thus, measures of regional lung mechanics can serve as a sensitive test of the status of the respiratory system and should be considerably more sensitive and informative than global pulmonary function test. Recent advances in multi-detector-row CT (MDCT), 4DCT respiratory gating methods, and image processing techniques enable us to study pulmonary function at the regional level with high resolution anatomical information compared to other methods. MDCT can be used to acquire multiple static breath-hold CT images of the lung taken at different lung volumes, or 4DCT images of the lung acquired during spiral scanning using a low pitch and retrospectively reconstructed at different respiratory phases with proper respiratory control [1, 2, 3]. Image registration can be applied to these data to estimate a deformation field that transforms the lung from one volume configuration to the other. This deformation field can be analyzed to estimate local lung tissue expansion, calculate voxel-by-voxel intensity change, and make biomechanical measurements. When combined with image segmentation algorithms [4, 5, 6, 7], functional and biomechanical measurements can be reported on a lung, lobe, and sublobar basis, and can be used to interpret regional lung function relative to specific segments of bronchial tree. Such measurements of pulmonary function have proven useful as a planning tool during RT planning [8, 9] and may be useful for tracking the progression of toxicity to nearby normal tissue during RT and can be used to evaluate the effectiveness of a treatment post-therapy [10].

Early studies using CT to study regional air volume changes have proved to enhance our understanding of normal lung function. Several groups have proposed methods that couple image registration and CT imaging to study regional lung function. Guerrero et al. have used optical-flow registration to compute lung ventilation from 4DCT [11, 12] with an intensity-based ventilation measure. Christensen et al. used image registration to match images across cine-CT sequences and estimate rates of local tissue expansion and contraction [13] using a Jacobian-based ventilation measure. While they were able to show that their accumulated measurements matched well with the global measurements, they were not able to compare the registration-based measurements to local measures of regional tissue ventilation. Recently, Castillo et al. compared the intensity-based and Jacobian-based calculations of ventilation from 4DCT with the ventilation from ^{99m}Tc -labeled aerosol SPECT/CT [14]. A statistically higher correlation to the SPECT/CT

1 based ventilation was found for intensity-based based calculation over the Jacobian-based
2 calculation. However, the comparison of the two techniques was based on the Dice sim-
3 ilarity coefficient between the thresholded masks within 20% variation from the 4DCT
4 and from SPECT/CT. Though their experiment is novel and important, since the average
5 mask size is about 490.5 mL (with average subject exhale volume 2452.7 mL, and 5 sub-
6 masks per subject), the comparison is more global than regional. In addition, as shown in
7 Section 2.4, both the intensity-based and Jacobian-based ventilation measures are based
8 on the assumption that regional lung volume change is due solely to air content change,
9 which may not always be a valid assumption. Other factors, such as blood volume change,
10 may also introduce the regional lung volume change.

11 The physiologic significance of these registration-based measures of respiratory function
12 can be established by comparing to more conventional measurements, such as nuclear
13 medicine or contrast wash-in/wash-out studies with CT or MR. Xenon-enhanced CT (Xe-
14 CT) measures regional ventilation by observing the gas wash-in or wash-out rate on serial
15 CT images [15, 16, 17] Xe-CT imaging has the advantage of high temporal resolution and
16 spatial resolution and reflects a measure of fresh gas delivery to the gas exchange units
17 of the lung. Although the dynamic Xe-CT method is limited in Z-axis coverage, requires
18 expensive Xe gas, and is technically challenging, it serves as the gold standard of regional
19 ventilation and can be used to compare with registration-based measures of regional lung
20 function in animal studies for validation purposes.

21 This paper describes three measures to estimate regional ventilation from image registra-
22 tion of CT images: the specific air volume change calculated from the Jacobian (SAJ); the
23 specific air volume change calculated by the corrected Jacobian (SACJ); and the specific
24 air volume change by intensity change (SAI). We show that the SAI ventilation measure
25 can be derived from the SAJ measure by making the assumption that there is no tissue
26 volume change between registration volumes. We evaluate these three measures by com-
27 paring them with a Xe-CT measure of ventilation in a regional basis ($20 \text{ mm} \times 20 \text{ mm}$
28 $\times 20 \text{ mm}$ cube, or 8 mL). Among these three registration based measures, we show that
29 the corrected Jacobian-based measure, SACJ, has the best correlation with the Xe-CT
30 derived measure of specific ventilation.

2 Material and methods

2.1 Method Overview

Our goal is to validate and compare the measures used to estimate regional lung ventilation from image registration by comparing them to Xe-CT estimated ventilation. Figure 1 shows a block diagram of the entire process. Two types of data were acquired for each animal: a 4DCT scan and a Xe-CT scan. In order to make our comparisons under the same physiological conditions, each animal was scanned and mechanically ventilated with the same respiratory rate, tidal volume (TV) and positive end-expiratory pressure (PEEP) during the two types of scans. The data sets from the 4DCT scan were reconstructed in volumes at eight phases of the respiratory cycle. For this study we focus on the data sets from two of the phases, a volume near end expiration (EE) and a volume near end inspiration (EI). For the Xe-CT scan, 45 distinctive partial lung volumetric scans were performed at volume near end expiration, or the initial end expiration scan (EE_0) to the last expiration scan (EE_{44}).

The nonlinear image registration is used to define the transformation T1 between the EE and EI in order to measure the regional lung ventilation from the 4DCT scan. The Xe-CT-based estimated regional lung ventilation is computed on the EE_0 by using Pulmonary Analysis Software Suite 11.0 (PASS) software by finding the constant of the exponential rise of the density from xenon gas wash-in over multiple breaths [18]. The same nonlinear image registration is also applied to define the transformation T2 which maps the EE_0 to the EE so that the Xe-CT based estimate of ventilation can be mapped into the same coordinate system as that of the registration-based estimate of ventilation. Additional details on the registration algorithm and other processing steps are given below.

2.2 Image Data Sets

Appropriate animal ethics approval was obtained for these protocols from the University of Iowa Animal Care and Use Committee and the study adhered to NIH guidelines for animal experimentation. Four adult male sheep A, B, C, and D (with weights 44.0, 37.8, 40.4, and 46.7 kg) were used for this study. The sheep were anesthetized using intravenous pentobarbital and pancuronium to ensure adequate sedation and to prevent spontaneous breathing. Animals were positive pressure ventilated during experiments using a custom built dual Harvard apparatus piston ventilator designed for computer control. The 4DCT images were acquired with the animals in the supine position using the dynamic imaging protocol with a pitch of 0.1, slice collimation of 0.6 mm, rotation time of 0.5 sec, slice

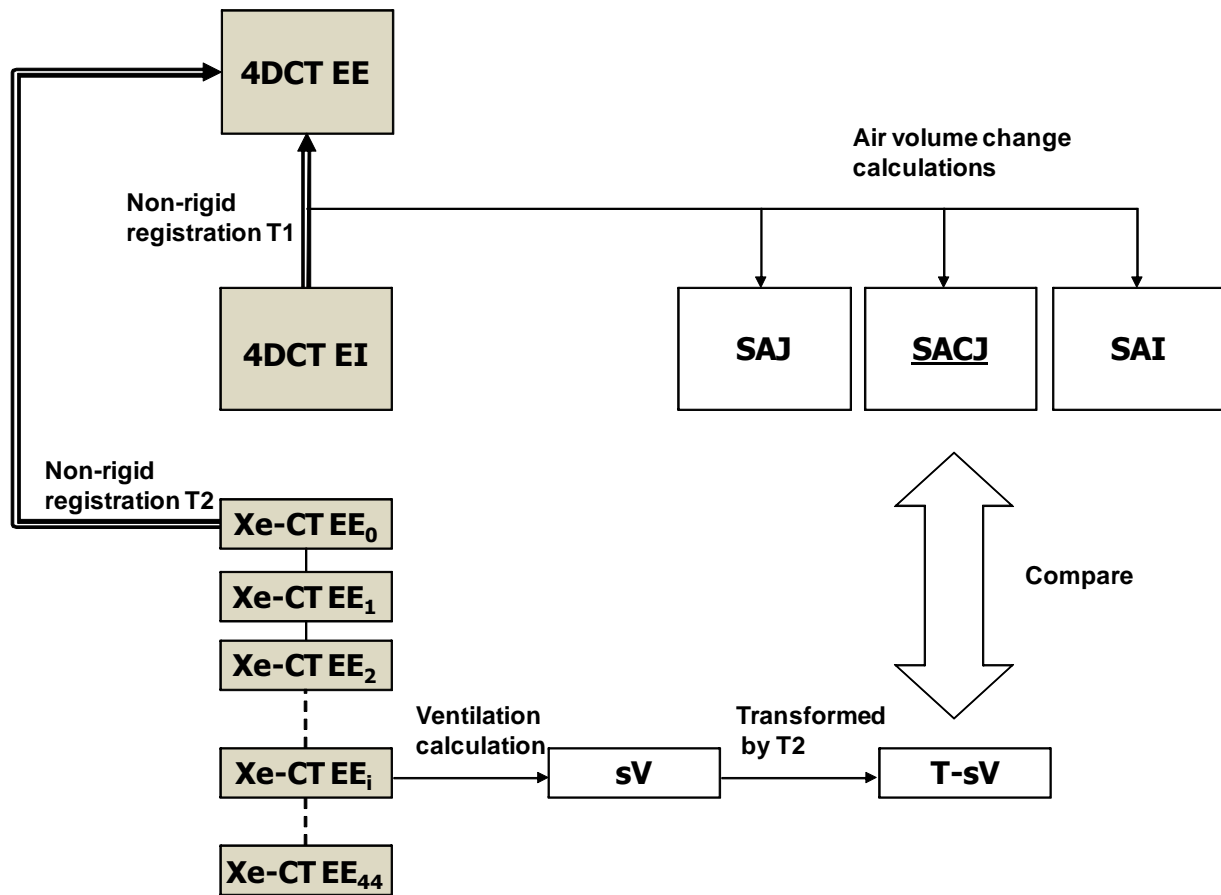


Figure 1: Figure shows the two types of images, a image pair of full lung volumetric phases EE and EI from a 4DCT scan and a Xe-CT scan acquired at end of expiration over 45 respiratory cycles (EE₀ to EE₄₄), which are analyzed during the processing. Transformation T1 registers end inspiration (EI) to end expiration (EE) data and can be used to assess local lung function via calculations of three ventilation measures: specific air volume change by specific volume change (SAJ), specific air volume change by corrected Jacobian (SACJ), and specific air volume change by intensity (SAI). The 45 distinctive partial lung volumetric Xe-CT scans EE₀ to EE₄₄ are used to calculate Xe-CT-based measure of specific ventilation (sV). Transformation T2 maps the sV data into the coordinate system of the EE image (end expiration phase of the 4DCT scan) to allow direct comparison with the 4DCT and registration-based measures of ventilation. Both EE and EE₀ are at volumes near end inspiration. (Shaded boxes indicate CT image data; white boxes indicated derived or calculated data; thick arrows indicate image registration transformations being calculated; thin solid lines indicate other operations.)

1 thickness of 0.75 mm, slice increment of 0.5 mm, 120 kV, 400 mAs, and kernel B30f. The
 2 airway pressure signal was simultaneously recorded with the X-ray projections and images
 3 were reconstructed retrospectively at 0, 25, 50, 75, and 100% of the inspiration duration
 4 and 75, 50 and 25% of the expiration duration. The 0% (EE) and 100% (EI) inspiration
 5 phases were used for later ventilation measurements. A slab of twelve contiguous axial
 6 slices were imaged over 45 breaths for Xe-CT scans. Images were acquired using respiratory
 7 gating by triggering the scan during end-expiration with 80 keV energy (for higher density
 8 resolution, approximately 2 HU per 1% Xe), 160 mAs tube current, a 360° rotation, a 0.33
 9 sec scan time, and 2.4 mm slice thickness. Respiratory gating is achieved using a custom
 10 built LabVIEW program which controls the ventilators and triggers the CT scanner. The
 11 respiratory rate (RR) for four animals ranged from 15 to 18 breaths per minute with an
 12 inspiratory-expiratory ratio of 1:1 which was sufficient to maintain a normocapnic state.
 13 Both of the two types of images were acquired with a matrix of 512 by 512 and without
 14 moving the animal between scans.

15 2.3 Image Registration

16 A tissue volume and vesselness measure preserving nonrigid registration (TVP) algo-
 17 rithm [19, 20] is used to estimate the transformations EI to EE and EE₀ to EE. The TVP
 18 algorithm minimizes the sum of squared tissue volume difference (SSTVD) [21, 22, 23, 24]
 19 and vesselness measure difference (SSVMD), utilizing the rich image intensity information
 20 and natural anatomic landmarks provided by the vessels. This method has been shown to
 21 be effective at registering across lung CT images with high accuracy [19, 20].

22 Let I_1 and I_2 represent two 3D image volumes to be registered. The vector $\mathbf{x} =$
 23 $(x_1, x_2, x_3)^T$ defines the voxel coordinate within an image. The algorithm finds the optimal
 24 transformation \mathbf{h} that maps the template image I_1 to the target image I_2 by minimizing
 25 the cost function

$$C_{\text{TOTAL}} = \rho \int_{\Omega} [V_2(\mathbf{x}) - V_1(\mathbf{h}(\mathbf{x}))]^2 d\mathbf{x} + \chi \int_{\Omega} [F_2(\mathbf{x}) - F_1(\mathbf{h}(\mathbf{x}))]^2 d\mathbf{x}. \quad (1)$$

26 where Ω is the union domain of the lung regions in images I_1 and I_2 . V_2 and V_1 are the
 27 tissue volumes as defined in Equation 2. F_2 and F_1 are the vesselness measures as defined
 28 in Equation 6. The transformation \mathbf{h} is a (3×1) vector-valued function that maps a point
 29 $\mathbf{h}(\mathbf{x})$ in the target image to its corresponding location in the template image. The first
 30 integral of the cost function defines the SSTVD cost and the second integral of the cost
 31 function defines the SSVMD cost.

1 The SSTVD cost assumes that the measured Hounsfield units (HU) in the lung CT
 2 images is a function of tissue and air content. Following the air-tissue mixture model by
 3 Hoffman et al. [25], from the CT value of a given voxel, the tissue volume can be estimated
 4 as

$$V(\mathbf{x}) = \nu(\mathbf{x}) \frac{I(\mathbf{x}) - HU_{air}}{HU_{tissue} - HU_{air}} = \nu(\mathbf{x})\beta(I(\mathbf{x})), \quad (2)$$

5 and the air volume can be estimated as

$$V'(\mathbf{x}) = \nu(\mathbf{x}) \frac{HU_{tissue} - I(\mathbf{x})}{HU_{tissue} - HU_{air}} = \nu(\mathbf{x})\alpha(I(\mathbf{x})), \quad (3)$$

6 where $\nu(\mathbf{x})$ denotes the volume of voxel \mathbf{x} and $I(\mathbf{x})$ is the intensity of a voxel at position \mathbf{x} .
 7 HU_{air} and HU_{tissue} refer to the intensity of air and tissue, respectively. In this work, we
 8 assume that air is -1000 HU and tissue is 0 HU. $\alpha(I(\mathbf{x})) = \frac{HU_{tissue} - I(\mathbf{x})}{HU_{tissue} - HU_{air}}$ and $\beta(I(\mathbf{x})) =$
 9 $\frac{I(\mathbf{x}) - HU_{air}}{HU_{tissue} - HU_{air}}$ are introduced for notational simplicity. Notice that $\alpha(I(\mathbf{x})) + \beta(I(\mathbf{x})) = 1$.
 10

Given (2), we can then define the SSTVD cost:

$$C_{\text{SSTVD}} = \int_{\Omega} [V_2(\mathbf{x}) - V_1(\mathbf{h}(\mathbf{x}))]^2 d\mathbf{x} \quad (4)$$

$$= \int_{\Omega} [\nu_2(\mathbf{x})\beta(I_2(\mathbf{x})) - \nu_1(\mathbf{h}(\mathbf{x}))\beta(I_1(\mathbf{h}(\mathbf{x})))]^2 d\mathbf{x}, \quad (5)$$

11 The notation $I_1(\mathbf{h}(\mathbf{x}))$ is interpreted as the image $I_1(\mathbf{x})$ deformed by the transformation
 12 $\mathbf{h}(\mathbf{x})$ and is computed using trilinear interpolation. The deformed volume element $\nu_1(\mathbf{h}(\mathbf{x}))$
 13 is calculated using the Jacobian $J(\mathbf{x})$ times the volume element $\nu_2(\mathbf{x})$, i.e., $\nu_1(\mathbf{h}(\mathbf{x})) =$
 14 $J(\mathbf{x})\nu_2(\mathbf{x})$.

15 Figure 2 shows an example of a cubic shaped region under deformation \mathbf{h} from template
 16 image to target image. The region volumes are ν_1 and ν_2 . The volumes can be decomposed
 17 into the tissue volume fraction and air volume fraction based on the mean voxel intensity
 18 within the cube. The small white sub volumes inside the cubes represent the tissue volume
 19 V_1 and V_2 . Air volumes are represented by V'_1 and V'_2 (in blue). As the ratio of air to
 20 tissue decreases, the CT intensity of a voxel increases. The mean cube voxel intensities for
 21 the template, I_1 , and target images, I_2 , are functions of the ratios of air to tissue volumes
 22 within the cubes.

23 As the blood vessels branch to smaller and smaller diameters, the raw grayscale in-
 24 formation from vessel voxels provide very little contribution to guide the intensity-based
 25 registration. To better utilize the information of blood vessel locations, we use the vessel-
 26 ness measure based on the eigenvalues of the Hessian matrix of image intensity. Frangi's

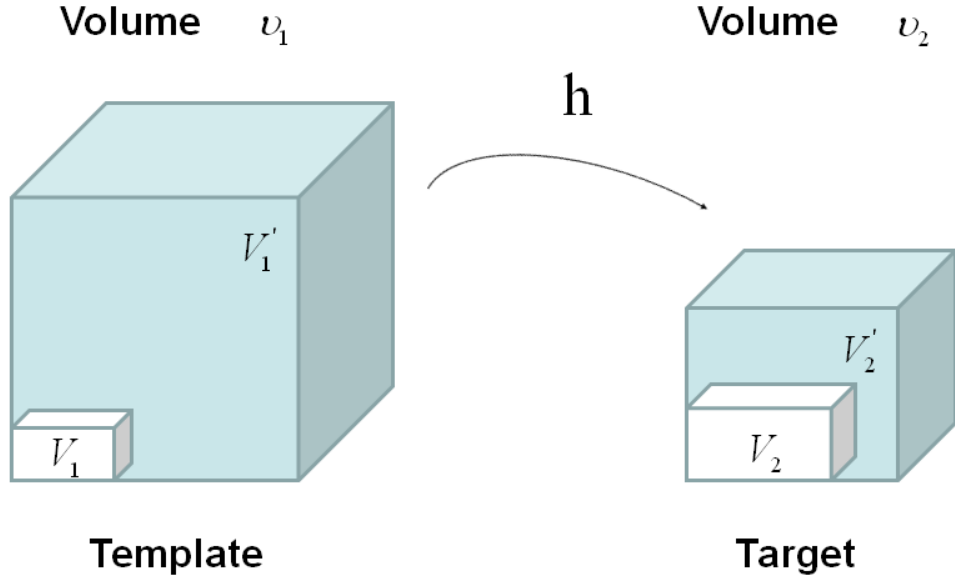


Figure 2: Example of a region under deformation $\mathbf{h}(\mathbf{x})$ from template image to target image. V_1 and V_2 are tissue volumes in the regions. V_1' and V_2' are air volumes in the regions. Region volumes $\nu_1 = V_1 + V_1'$ and $\nu_2 = V_2 + V_2'$.

1 vesselness function [26] is defined as

$$F(\lambda) = \begin{cases} (1 - e^{-\frac{R_A^2}{2\alpha^2}}) \cdot e^{-\frac{R_B^2}{2\beta^2}} \cdot (1 - e^{-\frac{S^2}{2\gamma^2}}) & \text{if } \lambda_2 < 0 \text{ and } \lambda_3 < 0 \\ 0 & \text{otherwise} \end{cases} \quad (6)$$

2 with

$$R_A = \frac{|\lambda_2|}{|\lambda_3|}, \quad R_B = \frac{|\lambda_1|}{\sqrt{|\lambda_2\lambda_3|}}, \quad S = \sqrt{\lambda_1^2 + \lambda_2^2 + \lambda_3^2}, \quad (7)$$

3 where R_A distinguishes between plate-like and tubular structures, R_B accounts for the
 4 deviation from a blob-like structure, and S differentiates between tubular structure and
 5 noise. The vesselness function has been previously widely used in vessel segmentations in
 6 lungs [27, 28] and in retinas [29]. α , β , γ control the sensitivity of the vesselness measure.
 7 The vesselness measure is rescaled to $[0, 1]$ and can be considered as a probability-like
 8 estimate of vesselness features. For this study, $\alpha = 0.5$, $\beta = 0.5$, and $\gamma = 5$ and the
 9 weighting constants in the total cost were set as $\rho = 1$ and $\chi = 0.2$. These parameters are
 10 similar to those used in our previous work [19, 20].

11 The transformation $\mathbf{h}(\mathbf{x})$ is a cubic B-splines transform:

$$\mathbf{h}(\mathbf{x}) = \mathbf{x} + \sum_{i \in G} \phi_i \beta^{(3)}(\mathbf{x} - \mathbf{x}_i), \quad (8)$$

1 where ϕ_i describes the displacements of the control nodes and $\beta^{(3)}(\mathbf{x})$ is a three-dimensional
 2 tensor product of basis functions of cubic B-Spline. A spatial multiresolution procedure
 3 from coarse to fine is used in the registration in order to improve speed, accuracy and
 4 robustness. The total cost in Equation 1 is optimized using a limited-memory, quasi-
 5 Newton minimization method with bounds (L-BFGS-B) [30] algorithm. The B-Splines
 6 coefficients are constrained so that the transformation maintains the topology using the
 7 sufficient conditions that guarantee the local injectivity of functions parameterized by
 8 uniform cubic B-Splines proposed by Choi and Lee [31].

9 2.4 Regional Ventilation Measures from Image Registration

10 After we obtain the optimal warping function $\mathbf{h}(\mathbf{x})$, we can calculate the regional ven-
 11 tilation, which is equal to the difference in local air volume change per unit time. The
 12 commonly-used ventilation measure is the specific ventilation sV which takes the initial
 13 air volume into account. The sV is equal to the specific air volume change $sVol$ per unit
 14 time. Or in other words, in a unit time,

$$sV = sVol = \frac{V'_1(\mathbf{h}(\mathbf{x})) - V'_2(\mathbf{x})}{V'_2(\mathbf{x})}. \quad (9)$$

15 Three different approaches for estimating (9) are described below:

16 **Specific air volume change by specific volume change (SAJ):** The SAJ regional
 17 ventilation measure is based on the assumption that local volume change is due to air
 18 volume change alone, and thus, any regional volume change is due only to local air volume
 19 change. Or, equivalently, the SAJ measure assumes that there is no tissue volume within
 20 the template or target volumes. Figure 3 illustrates such an assumption. Compared
 21 with the general condition in Figure 2, the region volume now is pure air volume, or
 22 equivalently, $\nu_1 = V'_1$ and $\nu_2 = V'_2$. In this case, the specific air volume change is equal
 23 to specific volume change. Since the Jacobian tells us the local volume expansion (or
 24 contraction), the regional ventilation can be measured by:

$$SAJ = \frac{\nu_1(\mathbf{h}(\mathbf{x})) - \nu_2(\mathbf{x})}{\nu_2(\mathbf{x})} = J(\mathbf{x}) - 1. \quad (10)$$

25 Previously, SAJ has been used as an index of the regional function and was compared
 26 with Xe-CT estimates of regional lung function [4]. Regional lung expansion, as estimated
 27 from the Jacobian of the image registration transformations, was well correlated with
 28 xenon CT specific ventilation [4, 6] (linear regression, average $r^2 = 0.73$).

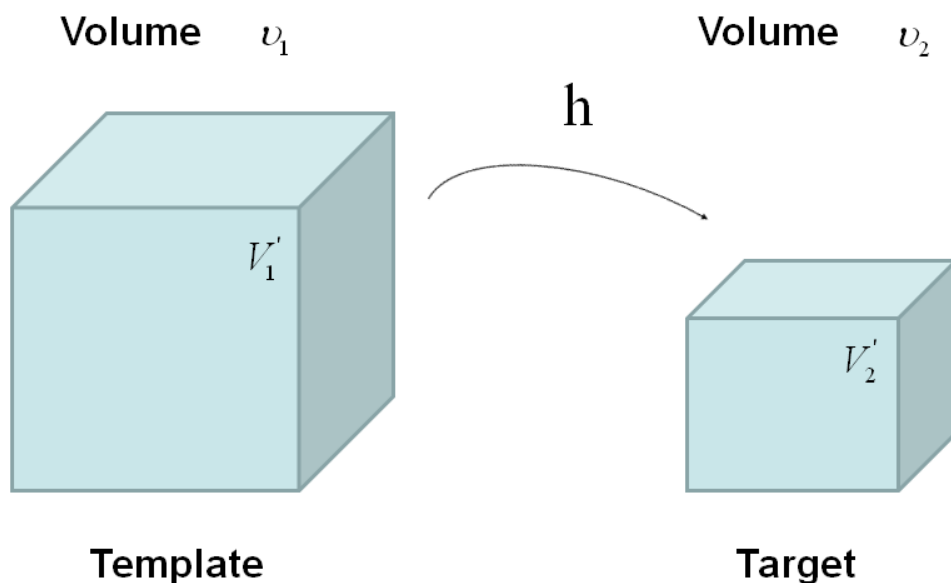


Figure 3: Example of a given region under deformation $\mathbf{h}(\mathbf{x})$ from template image to target image, with the assumption of no tissue volume ($V_1 = V_2 = 0$). V'_1 and V'_2 are air volumes.

- 1 **Specific air volume change by corrected Jacobian (SACJ):** Starting with (10)
 2 and expressing the air volumes $V'_1(\mathbf{h}(\mathbf{x}))$ and $V'_2(\mathbf{x})$ using the air-tissue mixture model (2)
 3 and (3), we obtain the corrected Jacobian measure of region air volume change, SACJ,

$$SACJ = \frac{V'_1(\mathbf{h}(\mathbf{x})) - V'_2(\mathbf{x})}{V'_2(\mathbf{x})} \quad (11)$$

$$= \frac{V'_1(\mathbf{h}(\mathbf{x}))}{V'_2(\mathbf{x})} - 1 \quad (12)$$

$$= \frac{\nu_1(\mathbf{h}(\mathbf{x}))\alpha(I_1(\mathbf{h}(\mathbf{x})))}{\nu_2(\mathbf{x})\alpha(I_2(\mathbf{x}))} - 1 \quad (13)$$

- 4 As $\nu_1(\mathbf{h}(\mathbf{x})) = J(\mathbf{x})\nu_2(\mathbf{x})$, the specific air volume change is then

$$SACJ = J(\mathbf{x})\frac{\alpha(I_1(\mathbf{h}(\mathbf{x})))}{\alpha(I_2(\mathbf{x}))} - 1 \quad (14)$$

$$= J(\mathbf{x})\frac{HU_{tissue} - I_1(\mathbf{h}(\mathbf{x}))}{HU_{tissue} - I_2(\mathbf{x})} - 1 \quad (15)$$

- 5 If we assume that pure air is -1000 HU and pure tissue is 0 HU, then specific air volume

1 change is

$$SACJ = J(\mathbf{x}) \frac{I_1(\mathbf{h}(\mathbf{x}))}{I_2(\mathbf{x})} - 1. \quad (16)$$

2 Compared to Equation 10, the term $\frac{I_1(\mathbf{h}(\mathbf{x}))}{I_2(\mathbf{x})}$ is a correction factor that depends on the
 3 voxel intensities in the template and target images. The SACJ measure is illustrated in
 4 Figure 2, and represents the most general case of where there is both tissue volume and
 5 air volume change within the region.

6 **Specific air volume change by intensity change (SAI):** The intensity-based mea-
 7 sure of regional air volume change SAI can be derived from the SACJ by assuming that
 8 tissue volume is preserved during deformation, or equivalently, that the tissue volume dif-
 9 ference $\Delta V(\mathbf{x}) = V_1(\mathbf{h}(\mathbf{x})) - V_2(\mathbf{x}) = 0$. Under this assumption, $V_1(\mathbf{h}(\mathbf{x})) = V_2(\mathbf{x})$ and we
 10 have

$$\nu_1(\mathbf{h}(\mathbf{x}))\beta(I_1(\mathbf{h}(\mathbf{x}))) = \nu_2(\mathbf{x})\beta(I_2(\mathbf{x})), \quad (17)$$

11 and

$$\nu_1(\mathbf{h}(\mathbf{x})) = \nu_2(\mathbf{x}) \frac{\beta(I_2(\mathbf{x}))}{\beta(I_1(\mathbf{h}(\mathbf{x})))}, \quad (18)$$

12 Since $\nu_1(\mathbf{h}(\mathbf{x})) = J(\mathbf{x})\nu_2(\mathbf{x})$, with above equation, we have

$$J(\mathbf{x}) = \frac{\beta(I_2(\mathbf{x}))}{\beta(I_1(\mathbf{h}(\mathbf{x})))} \quad (19)$$

$$= \frac{I_2(\mathbf{x}) - HU_{air}}{I_1(\mathbf{h}(\mathbf{x})) - HU_{air}}. \quad (20)$$

13 Substituting the above equation into equation 15, yields

$$SAI = \frac{I_2(\mathbf{x}) - HU_{air}}{I_1(\mathbf{h}(\mathbf{x})) - HU_{air}} \frac{HU_{tissue} - I_1(\mathbf{h}(\mathbf{x}))}{HU_{tissue} - I_2(\mathbf{x})} - 1 \quad (21)$$

$$= \frac{I_2(\mathbf{x})HU_{tissue} + HU_{air}I_1(\mathbf{h}(\mathbf{x})) - I_1(\mathbf{h}(\mathbf{x}))HU_{tissue} - HU_{air}I_2(\mathbf{x})}{(I_1(\mathbf{h}(\mathbf{x})) - HU_{air})(HU_{tissue} - I_2(\mathbf{x}))} \quad (22)$$

14 Finally, if we assume that pure air is -1000 HU and pure tissue is 0 HU, then

$$SAI = 1000 \frac{I_1(\mathbf{h}(\mathbf{x})) - I_2(\mathbf{x})}{I_2(\mathbf{x})(I_1(\mathbf{h}(\mathbf{x})) + 1000)} \quad (23)$$

15 which is exactly the result from Simon [32], Guerrero et al. [11], and Fuld et al. [33].

16 Figure 4 illustrates the assumption with no tissue volume change in SAI. In Figure 4

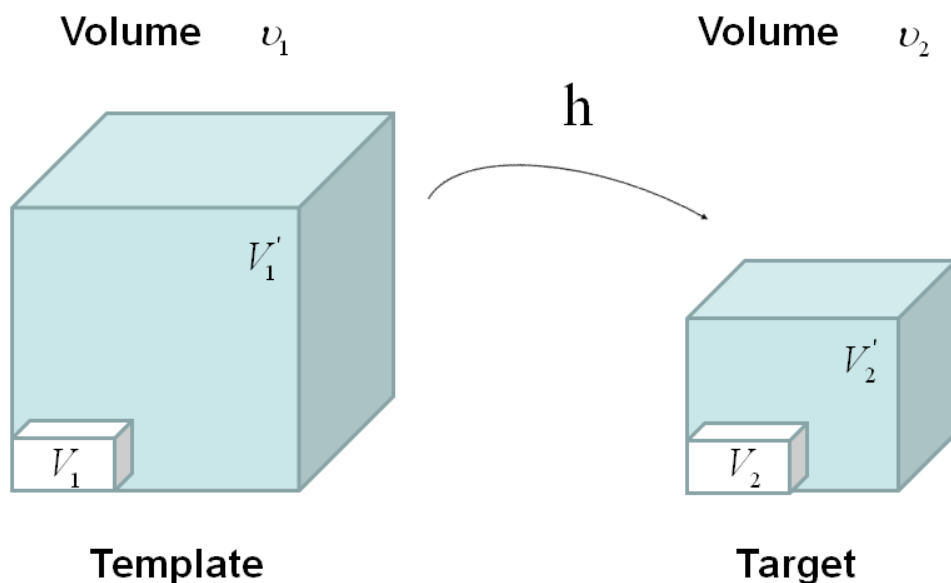


Figure 4: Example of a given voxel under deformation $\mathbf{h}(\mathbf{x})$ from template image to target image, with the assumption of no tissue volume change. Notice the tissue volume $V_1 = V_2$ under this assumption. V_1' and V_2' are air volumes.

1 as the region volume changes from ν_1 to ν_2 , the tissue volume inside the cube remains the
 2 same ($V_1 = V_2$).

3 **Difference of specific air volume change (DSA) and difference of tissue vol-**
 4 **ume (DT):** To investigate the relationship between the measurements of specific air
 5 volume changes and the tissue volume change, we can calculate the difference between
 6 equation (15) and equation (22) and define the difference of specific air volume change
 7 (DSA) between SACJ and SAI, and the difference of tissue volume (DT) as:

$$DSA = |SACJ - SAI| \quad (24)$$

$$DT = |V_1(\mathbf{h}(\mathbf{x})) - V_2(\mathbf{x})| \quad (25)$$

$$= |\nu_1(\mathbf{h}(\mathbf{x}))\beta(I_1(\mathbf{h}(\mathbf{x}))) - \nu_2(\mathbf{x})\beta(I_2(\mathbf{x}))| \quad (26)$$

$$= |J(\mathbf{x})\nu_2(\mathbf{x})\beta(I_1(\mathbf{h}(\mathbf{x}))) - \nu_2(\mathbf{x})\beta(I_2(\mathbf{x}))| \quad (27)$$

$$= |\nu_2(\mathbf{x}) \frac{J(\mathbf{x})(I_1(\mathbf{h}(\mathbf{x})) - HU_{air}) - (I_2(\mathbf{x}) - HU_{air})}{HU_{tissue} - HU_{air}}| \quad (28)$$

8 Again, if we assume that air is -1000 HU and tissue is 0 HU, then the tissue volume

1 difference is:

$$DT = |\nu_2(\mathbf{x}) \frac{J(\mathbf{x})(I_1(\mathbf{h}(\mathbf{x})) + 1000) - (I_2(\mathbf{x}) + 1000)}{1000}| \quad (29)$$

2 **2.5 Computational Setup**

3 Processing starts by identifying the lung regions in all images using the Pulmonary Work-
4 station 2.0 (VIDA Diagnostics, Inc., Iowa City, IA). The Xe-CT estimate of sV is computed
5 in the coordinates of the EE_0 using Pulmonary Analysis Software Suite 11.0 (PASS) [18] at
6 the original image size of $0.5 \text{ mm} \times 0.5 \text{ mm} \times 2.4 \text{ mm}$ voxels. Overlapping 1×8 regions
7 of interest (ROI) are defined in the lung region on each 2D slice. All images, including the
8 EE, EI, EE_0 and their corresponding lung region masks or sV map, are then resampled to
9 a voxel size of $1 \text{ mm} \times 1 \text{ mm} \times 1 \text{ mm}$. After preprocessing, EI is registered to EE using
10 the TVP registration for measuring the regional ventilation from these two phases in a
11 4DCT scan. The resulting transformation is used to estimate the SAJ, SACJ and SAI.
12 Then EE_0 is registered to EE using TVP registration as well to map the sV to the same
13 coordinate system as that of the SAJ, SACJ and SAI. Due to the fact that the denominator
14 of equation (15) and (22) may become zero, we eliminated from consideration any points
15 that have the absolute value of the denominator become less than 0.001. For the TVP
16 registration, the multiresolution strategy is used in the processing and it proceeds from
17 low to high image resolution starting at one-eighth the spatial resolution and increases by
18 a factor of two until the full resolution is reached. Meanwhile, a hierarchy of B-spline grid
19 spaces from large to small is used. The finest B-spline grid space used in the experiments
20 is 4 mm. The images and image grid space are refined alternatively.

21 **2.6 Assessment of image registration accuracy**

22 A semi-automatic landmark system is used for landmark selection and matching [34]. This
23 system first uses an automatic landmark detection algorithm to find the landmarks in the
24 EE image. The algorithm automatically detects “distinctive” points in the target image
25 as the landmarks based on a distinctiveness value $D(p)$. Around each point p , 45 points,
26 q_1, \dots, q_{45} are uniformly distributed on a spherical surface. A region of interest $ROI(q_i)$
27 is compared with the corresponding region of interest $ROI(p)$ around the original point,
28 and then combined with its gradient value to calculate the distinctiveness value $D(p)$.

29 The same system is then applied to guide the observer to match landmarks in the target
30 image with corresponding landmarks in the template image. Each landmark-pair manually
31 annotated by the observer is added to a thin-plate-spline to warp the template image. The
32 system utilizes the warped image to estimate where the anatomic match will be located

1 for a new landmark point presented to the observer, therefore the observer can start the
2 matching from a system estimated location. Thus, as the warped image becomes more
3 accurate by the new added landmarks, the task of the observer becomes easier.

4 For each animal, after 200 anatomic landmarks are identified in the EE image, the
5 observer marks the locations of the voxels corresponding to the anatomic locations of the
6 landmarks in the EI image. For each landmark, the actual landmark position is compared
7 to the registration-derived estimate of landmark position and the error is calculated. With
8 the evaluated accuracy of transformation from the lung image registration algorithm, the
9 resulting regional ventilation measures estimated using the transformation can be then
10 compared to Xe-CT estimated ventilation.

11 **2.7 Compare Registration Regional Ventilation** 12 **Measures to Xe-CT Estimated Ventilation**

13 In our previous work [4, 6], regional lung expansion, as estimated from the Jacobian of
14 the image registration transformations, was compared with Xe-CT-based sV. The analysis
15 was conducted by evaluating Jacobian value between a pair of lung volumes from static
16 (multiple airway pressures) and dynamic image data sets, and comparing the Jacobian
17 along the y (ventral-dorsal) axis. While the correlation between the Jacobian value and
18 sV reflect the fact that regional expansion estimated from image registration can be used
19 as an index as regional lung function, the spatial resolution of the analysis method em-
20 ployed were likely not sufficient to distinguish the differences between regional ventilation
21 measures as we have described in Section 2.4. Therefore, to locally compare the regional
22 ventilation measures, the corresponding region of Xe-CT image EE_0 in the EE is divided
23 into approximately 100 non-overlapping cubes with size of $20 \text{ mm} \times 20 \text{ mm} \times 20 \text{ mm}$.
24 We compare the average regional ventilation measures (SAJ, SACJ and SAI) to the corre-
25 sponding average sV measurement from Xe-CT images within each cube. The correlation
26 coefficients between any two estimates (SAJ-sV, SACJ-sV or SAI-sV) are calculated by
27 linear regression. To compare two correlation coefficients, the Fisher Z-transform of the r
28 values is used and the level of significance is determined [35]. The relationship between the
29 specific air volume change and difference of tissue volume is also studied in four animals
30 by linear regression analysis.

3 Results

3.1 Registration Accuracy

For each animal, approximately 200 automatically identified landmarks within the lungs are used to compute registration accuracy. The landmarks are widely distributed throughout the lung regions. Figure 5 shows an example of the distribution of the landmarks in animal D for both the EE and EI images. The coordinate of each landmark location is recorded for each image data set before and after registration for all four animals. Figure 6 shows the landmark distance before and after registration for four animals. The grey boxes show the magnitude of respiratory motion during the tidal breathing. For all four animals, before registration, the average landmark distance is 6.6 mm with a minimum distance of 1.0 mm, maximum distance of 14.6 mm, and standard deviation of 2.42 mm. After registration, the average landmark distance is 0.4 mm with a minimum distance of 0.1 mm, a maximum distance of 1.6 mm, and a standard deviation 0.29 mm. The trends for all animals are consistent and the results demonstrate that the registrations produced good anatomic correspondences. All registrations were examined and it was confirmed that all Jacobian values had positive values.

Figure 5(a) shows the location of the EE_0 (Xe-CT) slab overlaid on the EE image. Figure 7 shows an example of the image registration result from the EE_0 image to the EE image. The first row shows the misalignment between the images before image registration. Though the images were acquired without moving the animal between the scans, there is still non-rigid deformation between scans as shown in Fig 7(d), as the black and white regions represent the large intensity difference between Fig. 7(a) and (b). In addition, the slice thicknesses were quite different which causes partial volume artifacts. After image registration, the EE_0 image is aligned to the EE image, and the resulting difference image (shown in Fig. 7(e)) is near zero. The transformation from the EE_0 to the EE image allows us to map the Xe-CT sV into the coordinate system of EE image. Note that since the regions outside the lung are not included in the registration process, the mediastinum and other body tissues are not aligned. Also note that the dorsal region of the lung shows a intensity difference after registration. This is due mainly to the gradual progression of atelectasis and tissue edema during the course of the experiment.

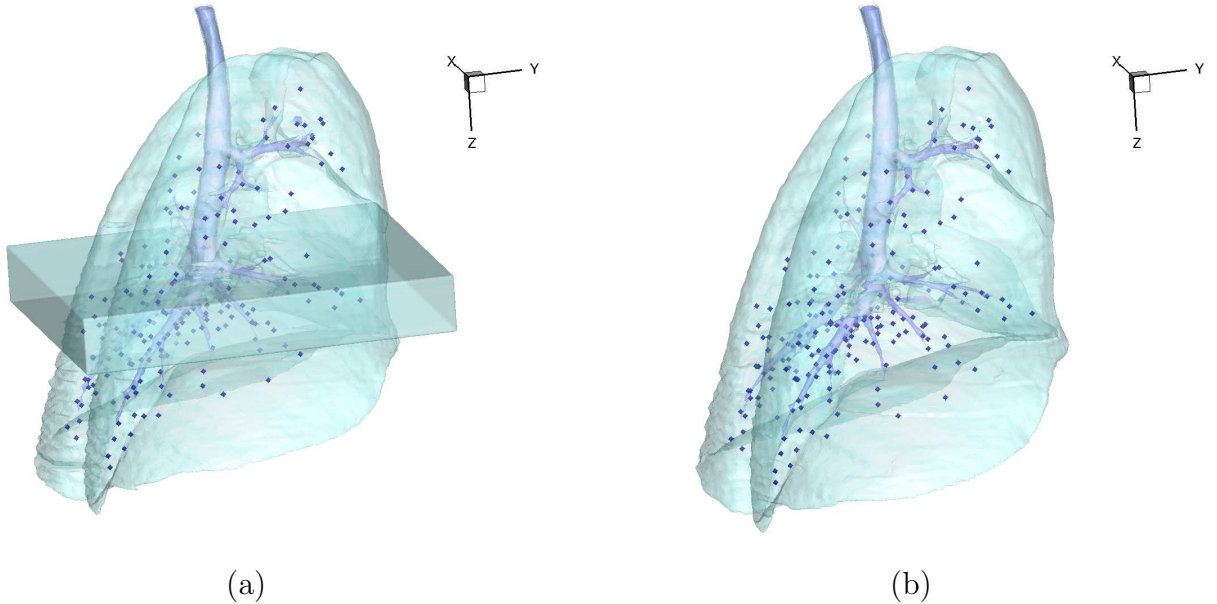


Figure 5: 3D view of the landmarks in: (a) EE with EE_0 and (b) EI. The dark region below the carina in (a) is the EE_0 and the spheres are the automatically defined landmarks.

3.2 Registration Estimated Ventilation Compared to Xe-CT Estimated Ventilation

Figure 8(a) shows a comparison between the registration-derived indices of ventilation and the Xe-CT estimated sV in cube-shaped regions of interest for animal D. The corresponding Xe-CT regions in the EE are divided into about 100 cubes. Figure 8(b) is the Xe-CT estimate of sV. Figure 8(c), (d), (e) are the corresponding registration ventilation measures SAJ, SACJ and SAI. The regions with edema are excluded from the comparison. Figure 8(b) to (d) all show noticeable similar gradient in the ventral-dorsal direction. Notice that the color scales are different in each map and are set based on the range of values from the appropriate plot in Fig. 9.

Figure 9 shows scatter plots comparing the registration ventilation measures and the Xe-CT ventilation sV in all four animals. The SACJ column shows the strongest correlation with the sV (average $r^2 = 0.82$). The SAJ, which is directly related to Jacobian as $SAJ = J - 1$, also shows good correlation with the sV (average $r^2 = 0.75$). The intensity-based measure SAI shows the lowest correlation with the sV (average $r^2 = 0.58$).

Table 1 shows the results of comparing the r values from SACJ vs. sV and SAI vs. sV. All four animals show that the correlation coefficient from SACJ vs. sV is significantly stronger than it from SAI vs. sV. Similarly, table 2 shows the results of comparing the r values from SAJ vs. sV and SAI vs. sV. The registration ventilation measure SAJ also

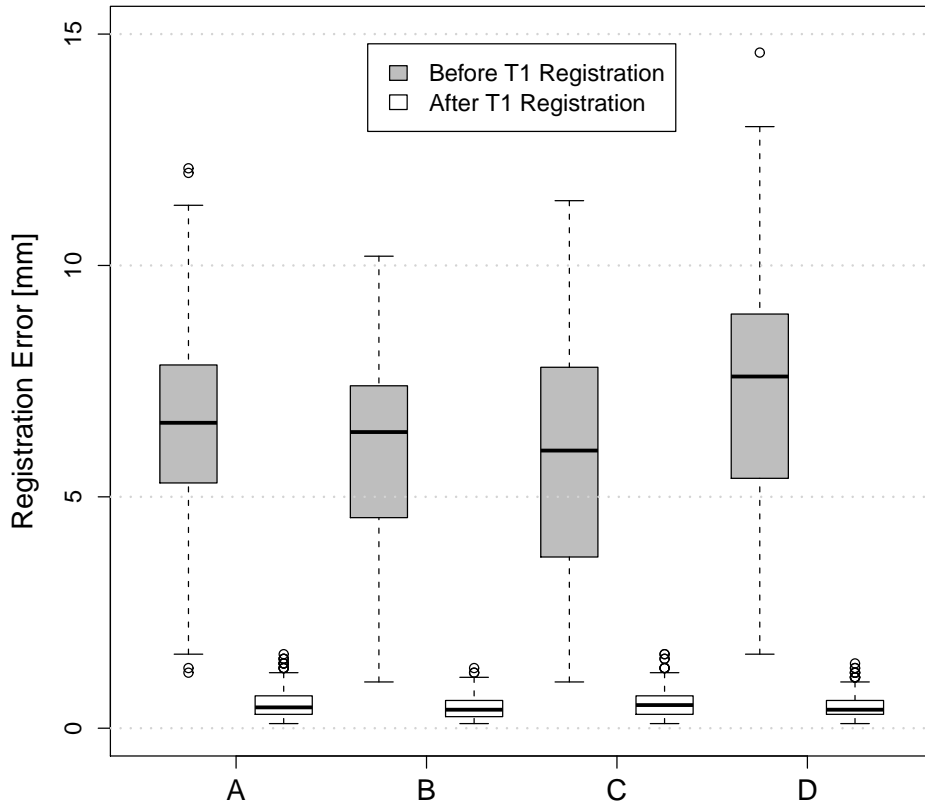
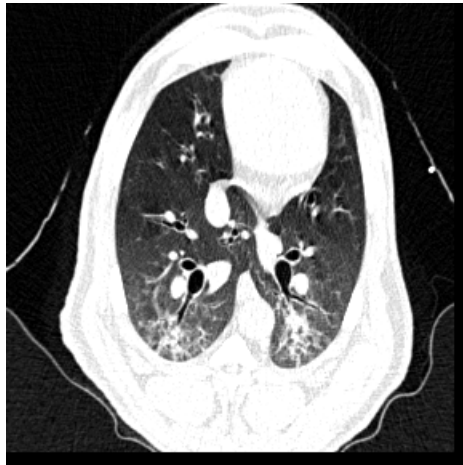
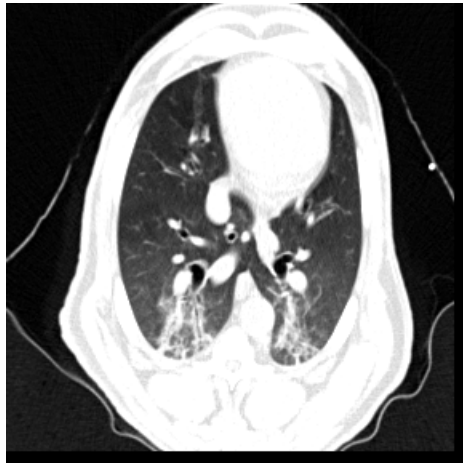


Figure 6: Landmarks distances of the registration pair EI to EE for all four animals. Boxplot lower extreme is first quartile, boxplot upper extreme is third quartile. Median is shown with solid horizontal line. Whiskers show either the minimum (maximum) value or extend 1.5 times the first to third quartile range beyond the lower (upper) extreme of the box, whichever is smaller (larger). Outliers are marked with circles.



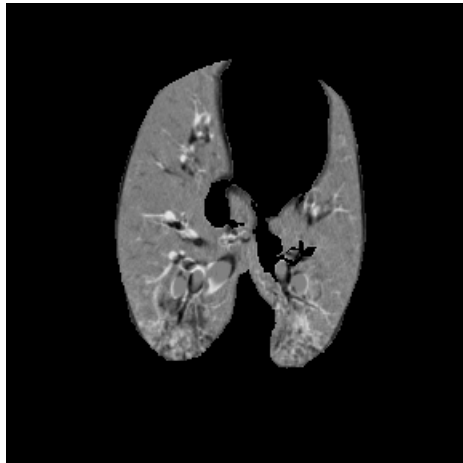
(a)



(b)



(c)



(d)



(e)

Figure 7: Visualization of the result of the transformation that maps the Xe-CT estimated ventilation sV to the EE coordinate system: (a) EE, (b) EE_0 , (c) deformed EE_0 after registration, (d) intensity difference between EE and EE_0 before registration, (e) intensity difference between EE and EE_0 after registration.

1 shows a significantly stronger correlation with sV than SAI. Comparing the r values from
2 SACJ vs. sV and SAJ vs. sV, only animal B and C show that the SACJ has significantly
3 stronger correlation with sV than SAJ.

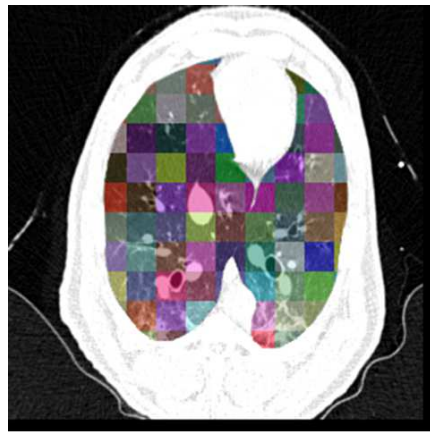
4 To analyze the effect of the size of the region of interest, the corresponding region
5 of Xe-CT image EE_0 in the EE is divided into about 30 slabs along the ventral-dorsal
6 direction with size of $150 \text{ mm} \times 8 \text{ mm} \times 40 \text{ mm}$ as similarly in our previous work [4, 6].
7 Figure 10 shows the scatter plots between the registration ventilation measures and the
8 Xe-CT ventilation sV similar as Fig. 10 but in larger ROIs. The SACJ column shows
9 the strongest correlation with the sV (average $r^2 = 0.92$). Both the SAJ and SAI show
10 good correlation with sV as well (average $r^2 = 0.88$ and $r^2 = 0.87$). However, though
11 the average r^2 value still show the SACJ has the highest correlation with Xe-CT based
12 sV, Table 4 and 5 show that with larger averaging region as defined slabs, there is no
13 significant difference between the correlation coefficients from SACJ vs. sV and SAI vs.
14 sV, between SAJ vs. sV and SAI vs. sV, or SACJ vs. sV and SAJ vs. sV as in Table 6.

15 Figure 11 shows the scatter plots between DSA (the absolute difference of the value
16 between the SACJ and SAI) and the DT (the absolute difference of the tissue volume)
17 with linear regression in all four animals (average $r^2 = 0.86$). From the equation (15)
18 and (22), we know that the SAI measurement assumes no tissue volume change in a given
19 region being registered, which may not be valid assumption in all lung regions. Figure 11
20 shows that as the tissue volume change increases, the difference between the measures of
21 regional ventilation from SACJ and SAI increases linearly in all four animals. It indicates
22 that the lower correlation of SAI with sV compared with SACJ with sV may be caused
23 by the tissue volume change between two volumes.

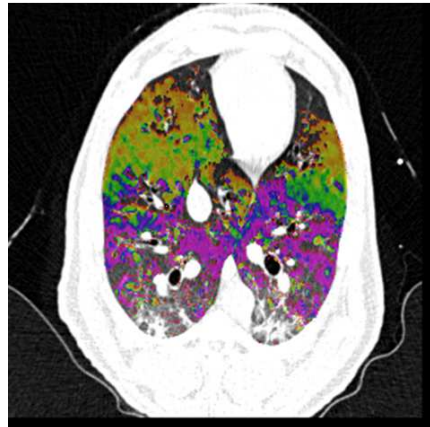
24 4 Summary and Conclusions

25 We described three measures to estimate regional lung tissue ventilation from tissue volume
26 and vesselness preserving image registration of CT images. These measures have been
27 compared with each other, and compared to Xe-CT estimates of specific ventilation. We
28 examined the assumption of constant tissue volume between registered lung regions, and
29 demonstrated that the difference between two of the registration derived measures (SACJ
30 and SAI) may be explained by differences in tissue volume between the lung regions being
31 compared with registration.

32 The tissue volume and vesselness preserving non-linear registration algorithm was used
33 to match the EI image to the EE image to produce the registration deformation field and
34 estimates of regional ventilation. It was used to register the EE_0 image to the EE image for

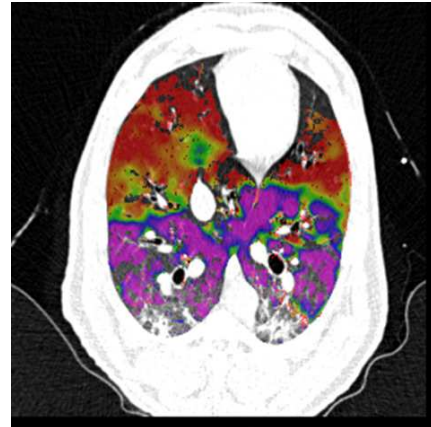


(a)



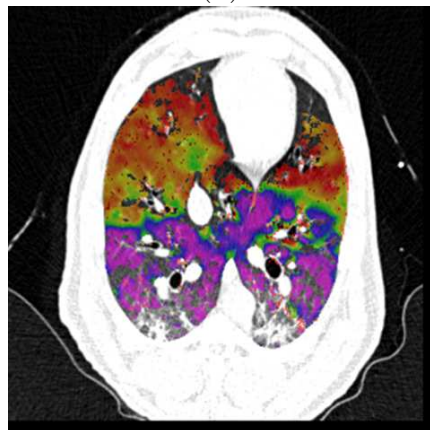
0.0 1.0 2.0 3.0 4.0 5.0 6.0

(b)



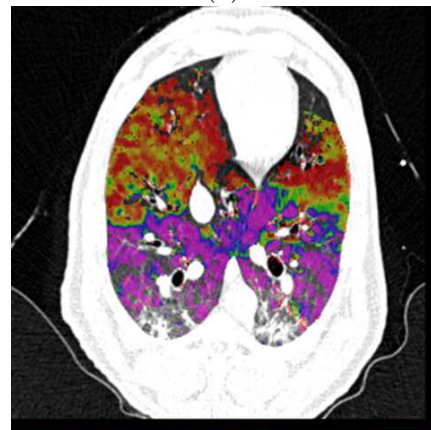
0.0 1.2 2.3 3.5 4.7 5.9 7.0

(c)



0.0 1.8 3.6 5.5 7.3 9.1 11.0

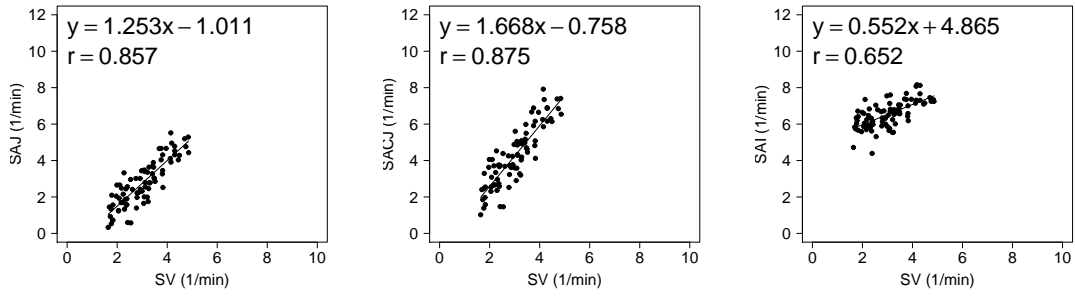
(d)



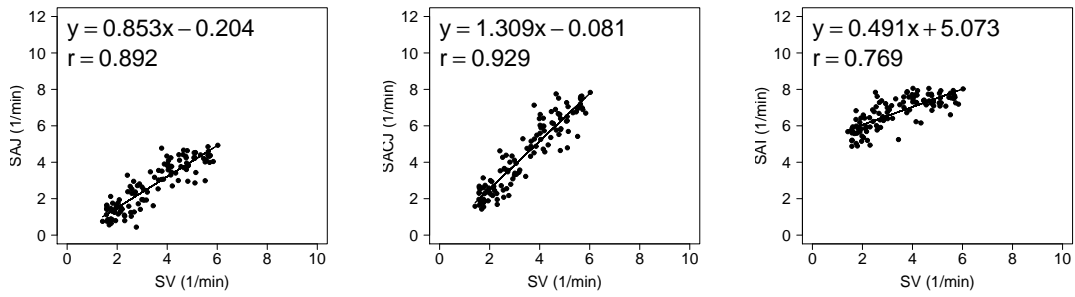
0.0 1.8 3.6 5.5 7.3 9.1 11.0

(e)

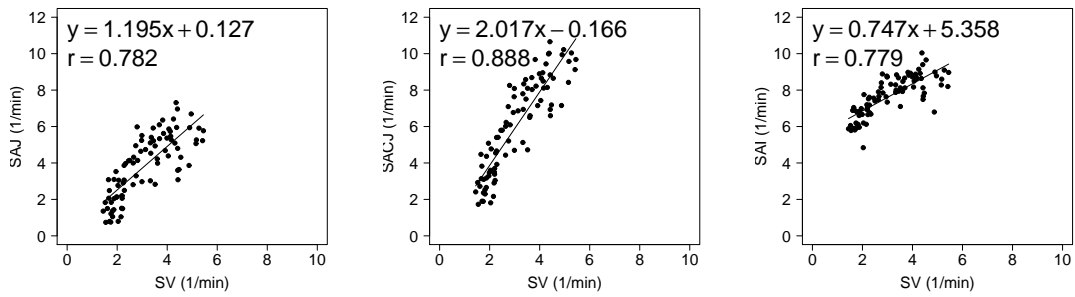
Figure 8: Comparison of the regional ventilation measures for animal D. (a): EE with color coded cubes showing the sample region. (b), (c), (d) and (e): color map of the sV, SAJ, SACJ and SAI. Note that the color scales are different for (b)-(e), and are set based on the range of values from the appropriate plot in Fig. 9. The results were similar for the other three animals



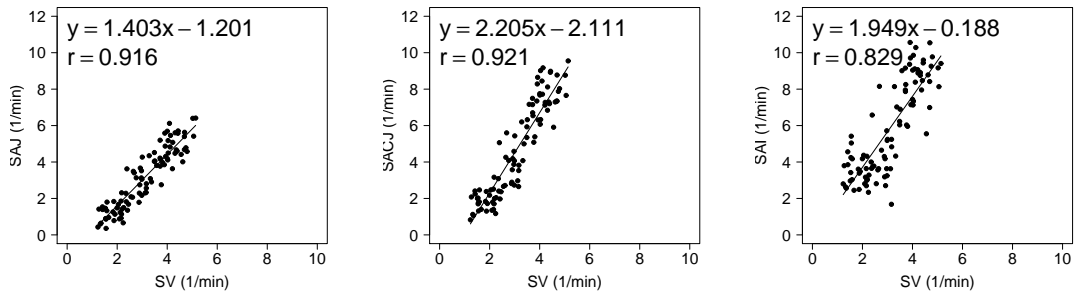
Animal A



Animal B

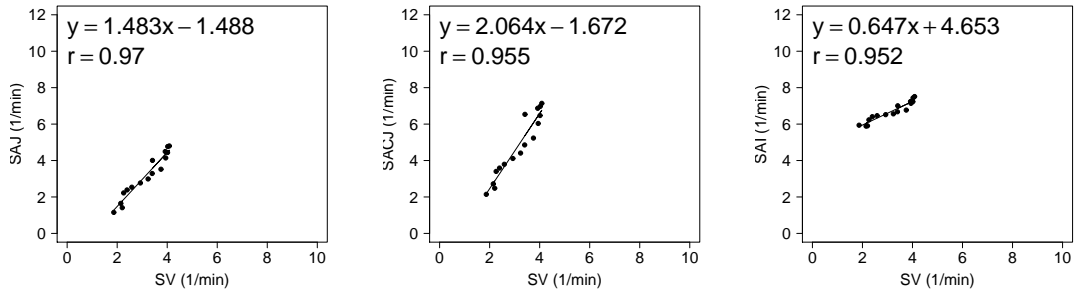


Animal C

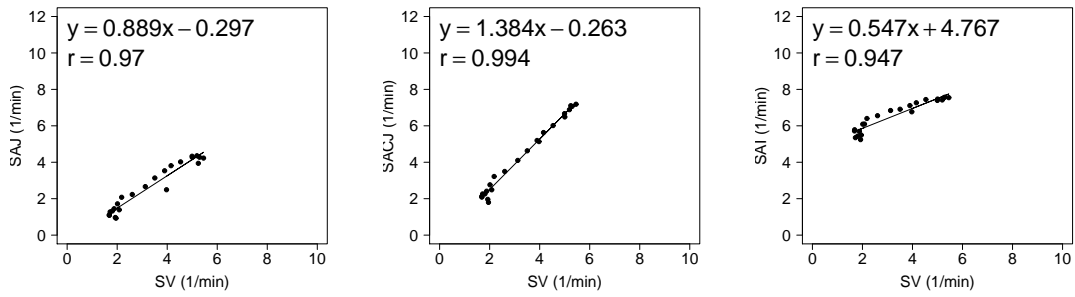


Animal D

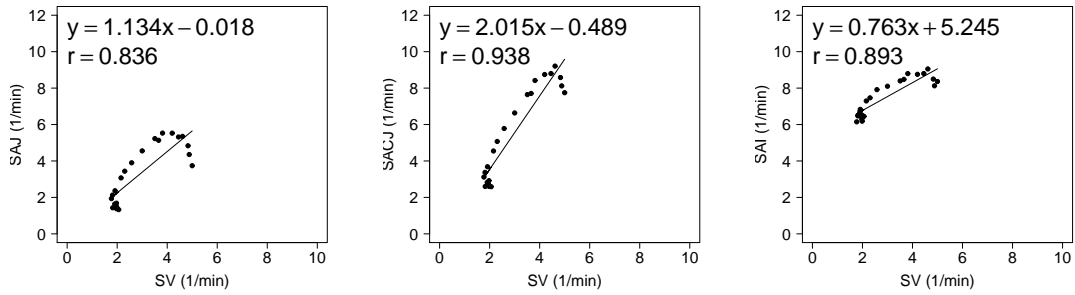
Figure 9: Small cube ROIs with size 20 mm × 20 mm × 20 mm results for registration estimated ventilation measures compared to the Xe-CT estimated ventilation sV in scatter plot with linear regression in four animals. The first column is the SAJ vs. sV. The second column is the SACJ vs. sV. The third column is the SAI vs. sV.



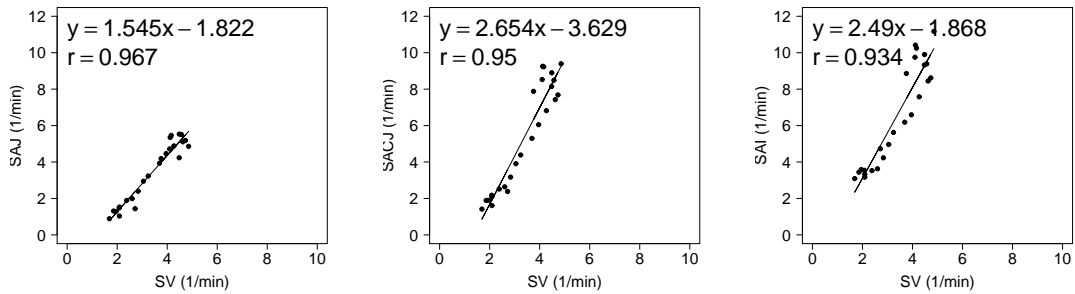
Animal A



Animal B



Animal C



Animal D

Figure 10: Large slab ROIs with size 150 mm × 8 mm × 40 mm results for registration estimated ventilation measures compared to the Xe-CT estimated ventilation sV in scatter plot with linear regression in four animals. The first column is the SAJ vs. sV. The second column is the SACJ vs. sV. The third column is the SAI vs. sV.

Animal	Correlation pair	Correlation with sV (r value)	Number of samples	SACJ vs. SAI p value
A	SACJ vs. sV	0.88	83	$p \leq 0.0001$
	SAI vs. sV	0.65		
B	SACJ vs. sV	0.93	119	$p \leq 1.18e^{-6}$
	SAI vs. sV	0.77		
C	SACJ vs. sV	0.89	86	$p \leq 0.0075$
	SAI vs. sV	0.78		
D	SACJ vs. sV	0.92	110	$p \leq 0.0017$
	SAI vs. sV	0.83		

Table 1: Comparison of ventilation measures between SACJ and SAI in small cube ROIs with size 20 mm \times 20 mm \times 20 mm.

Animal	Correlation pair	Correlation with sV (r value)	Number of samples	SAJ vs. SAI p value
A	SAJ vs. sV	0.86	83	$p \leq 0.0005$
	SAI vs. sV	0.65		
B	SAJ vs. sV	0.89	119	$p \leq 0.002$
	SAI vs. sV	0.77		
C	SAJ vs. sV	0.78	86	$p \leq 0.5$
	SAI vs. sV	0.78		
D	SAJ vs. sV	0.92	110	$p \leq 0.0017$
	SAI vs. sV	0.83		

Table 2: Comparison of ventilation measures between SAJ and SAI in small cube ROIs with size 20 mm \times 20 mm \times 20 mm.

Animal	Correlation pair	Correlation with sV (r value)	Number of samples	SACJ vs. SAJ p value
A	SACJ vs. sV	0.88	83	$p \leq 0.302$
	SAJ vs. sV	0.86		
B	SACJ vs. sV	0.93	119	$p \leq 0.035$
	SAJ vs. sV	0.89		
C	SACJ vs. sV	0.89	86	$p \leq 0.007$
	SAJ vs. sV	0.78		
D	SACJ vs. sV	0.92	110	$p \leq 0.5$
	SAJ vs. sV	0.92		

Table 3: Comparison of ventilation measures between SACJ and SAJ in small cube ROIs with size 20 mm \times 20 mm \times 20 mm.

Animal	Correlation pair	Correlation with sV (r value)	Number of samples	SACJ vs. SAI p value
A	SACJ vs. sV	0.95	17	$p \leq 0.5$
	SAI vs. sV	0.95		
B	SACJ vs. sV	0.99	23	$p \leq 0.005$
	SAI vs. sV	0.95		
C	SACJ vs. sV	0.94	23	$p \leq 0.15$
	SAI vs. sV	0.89		
D	SACJ vs. sV	0.95	25	$p \leq 0.28$
	SAI vs. sV	0.93		

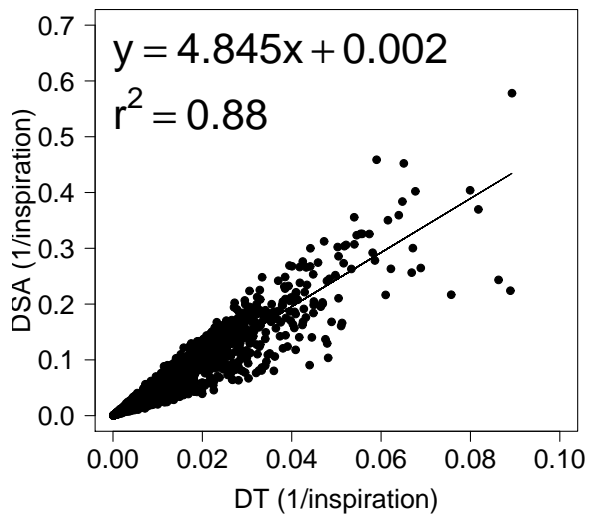
Table 4: Comparison of ventilation measures between SACJ and SAI in large slab ROIs with size 150 mm \times 8 mm \times 40 mm.

Animal	Correlation pair	Correlation with sV (r value)	Number of samples	SAJ vs. SAI p value
A	SAJ vs. sV	0.95	17	$p \leq 0.5$
	SAI vs. sV	0.95		
B	SAJ vs. sV	0.99	23	$p \leq 0.005$
	SAI vs. sV	0.95		
C	SAJ vs. sV	0.94	23	$p \leq 0.16$
	SAI vs. sV	0.89		
D	SAJ vs. sV	0.95	25	$p \leq 0.28$
	SAI vs. sV	0.93		

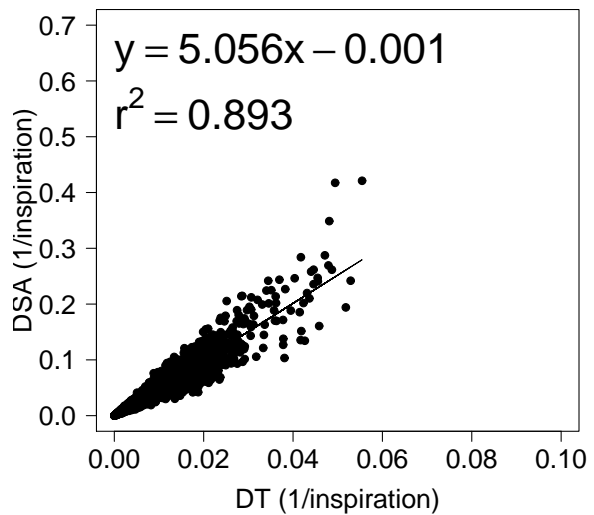
Table 5: Comparison of ventilation measures between SAJ and SAI in large slab ROIs with size 150 mm \times 8 mm \times 40 mm.

Animal	Correlation pair	Correlation with sV (r value)	Number of samples	SACJ vs. SAI p value
A	SACJ vs. sV	0.95	17	$p \leq 0.5$
	SAJ vs. sV	0.95		
B	SACJ vs. sV	0.99	23	$p \leq 0.5$
	SAJ vs. sV	0.99		
C	SACJ vs. sV	0.94	23	$p \leq 0.5$
	SAJ vs. sV	0.94		
D	SACJ vs. sV	0.95	25	$p \leq 0.5$
	SAJ vs. sV	0.95		

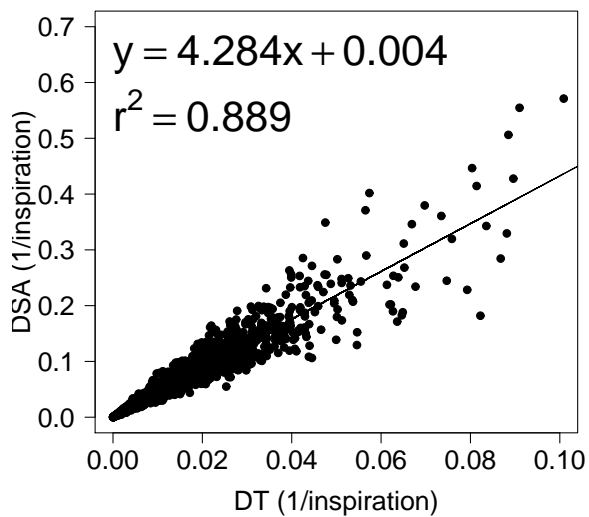
Table 6: Comparison of ventilation measures between SACJ and SAJ in large slab ROIs with size 150 mm \times 8 mm \times 40 mm.



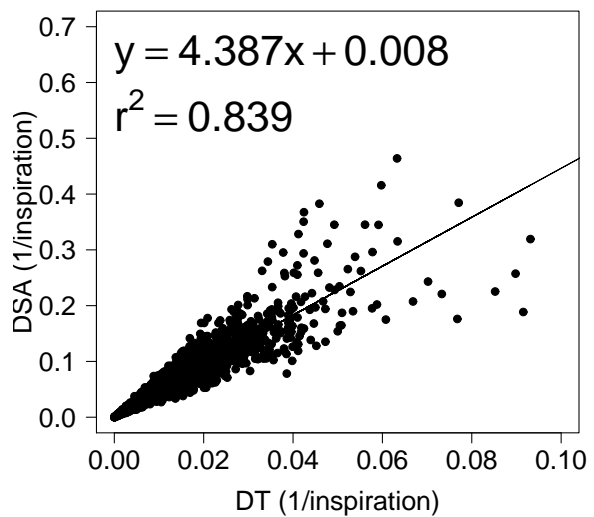
(a)



(b)



(c)



(d)

Figure 11: Linear regression analysis between DSA and DT. (a) to (d): DSA (the absolute difference of the value between the SACJ and SAI) compared to DT (the absolute difference of the tissue volume) in animals A, B, C and D.

1 comparing the three ventilation measures to the Xe-CT based sV. About 200 anatomical
2 landmarks were identified and annotated in each data set to evaluate registration accuracy.
3 The average landmark error is on the order of 1 mm after registration.

4 The ventilation measures SAJ, SACJ, and SAI were derived using a simple model of a
5 lung region, containing a mixture of air and tissue, which deforms during inspiration or
6 exhalation. The SAJ measure, which is a linear function of the Jacobian of the registration
7 displacement field, measures regional ventilation based on the assumption that the lung
8 region contains only air (i.e., no tissue volume). The SACJ is the most general form of
9 the three measures and is based on model where both the air and tissue volumes can
10 change during inspiration and exhalation. Finally, the SAI measure is computed based on
11 intensity change alone, and assumes that the region may have a tissue volume that is non-
12 zero, but this volume does not change during inspiration and exhalation. Thus, the SAJ
13 measure relies solely on the volume change information computed from the Jacobian of
14 the deformation field and the SAI measure relies solely on the change in region intensity as
15 measured by the CT. The SACJ measure uses a more complete model of local ventilation,
16 and combines the geometric information from the Jacobian with the density information
17 calculated from the change in region intensity.

18 The three registration-based ventilation measures and the Xe-CT sV measurement were
19 averaged and compared in cubic-shaped regions of interest. In $20 \text{ mm} \times 20 \text{ mm} \times 20$
20 mm ROIs, the SACJ shows significantly higher correlation with Xe-CT sV than the SAI
21 in all four animals. By studying the difference between the SACJ and SAI measures and
22 the tissue volume difference estimated by the CT intensity change, we showed that the
23 difference between SACJ and SAI may be explained by the constant tissue volume as-
24 sumption implicit in the SAI model (19). From Fig. 11, we see that the difference between
25 the SACJ and SAI measures is approximately linearly-related to the estimated tissue vol-
26 ume change. Tables 1 and 2 show that the both the SACJ and SAJ have significantly
27 better correlation with sV than the SAI. This is consistent with the findings by Kabus
28 et al. [36] who showed that the Jacobian-based measure of ventilation has less error than
29 the intensity-based ventilation measure, using the segmented total lung volume as a global
30 comparison. Though all the regional ventilation measures and Xe-CT based sV from the
31 linear regression analysis in Fig. 10 show high correlations, Tables 4 and 5 show that
32 there is no significant difference in the correlation with sV between the Jacobian-based
33 measures and intensity-based measure. This result indicates that the validation methods
34 using global comparison such as segmented total volume may not be able to distinguish
35 the Jacobian-based measure and the intensity-based measure.

36 The comparison of the ventilation measures was limited to the resolution of $20 \text{ mm} \times$

1 20 mm \times ROIs. As the size of the ROIs decreases, the correlation between the ventilation
2 measures with Xe-CT based sV decreases. This may be due to the underlying noise of
3 the Xe-CT measurement of ventilation or the decreased sensitivity of registration based
4 measure to local ventilation heterogeneity which is relative to the case. Additional Xe-CT
5 image analysis work including using multi-compartment models, thinner slice, and inter-
6 phase registration to improve sV measurement are required to reduce the noise in Xe-CT
7 based sV measurement.

8 To compare with the intensity-based ventilation measure used in previous work in Si-
9 mon [32], Guerrero et al. [11], and Fuld et al. [33], we followed the assumption that HU_{air}
10 is -1000 HU and HU_{tissue} is 0 HU (equaling water [25]) in this work. The ventilation mea-
11 sures were calculated under the assumption that HU_{air} is -1000 HU and HU_{tissue} is 55 HU,
12 which are the values used by Yin et al. in [22]. Our analysis shows that the correlation
13 coefficients between any two estimates (SAJ-sV, SACJ-sV or SAI-sV) change less than
14 1% with two different HU_{tissue} values. However, it would be important to have sensitivity
15 analysis in the future to compare different ventilation measures against intensity changes.

16 The image registration algorithm used to find the transformation from EI to EE for
17 measurement of regional ventilation produces accurate registrations by minimizing the
18 tissue volume and vesselness measure difference between the template image and the target
19 image. It would be interesting to compare different image registration algorithms and their
20 effects on the registration-based ventilation measures. For example, if two registration
21 algorithms achieve the similar landmark accuracy, the one does not preserve tissue volume
22 change may show even larger difference in the SACJ and SAI measures than the results
23 using TVP as described above.

24 In conclusion, with the same deformation field by the same image registration algorithm,
25 a significant difference between the Jacobian/-corrected Jacobian-based ventilation mea-
26 sures and the intensity-based ventilation measure is found in a regional level using Xe-CT
27 based ventilation measure sV. The ventilation measure by corrected Jacobian SACJ gives
28 best correlation with Xe-CT based sV and the correlation is significantly higher than from
29 the ventilation by intensity SAI indicating the ventilation measure by corrected Jacobian
30 SACJ may be a better measure of regional lung ventilation from image registration of
31 4DCT images.

32 5 Acknowledgments

33 The authors would like to thank Ms. K. Murphy and Dr. B. van Ginneken for providing
34 the software iX for generating and annotating landmarks. This work was supported in

1 part by NIH grant HL079406 and EB004126.

2 References

- 3 [1] P. J. Keall, V. R. Kini, S. S. Vedam, and R. Mohan, “Potential radiotherapy im-
4 provements with respiratory gating,” *Australasian physical & engineering sciences in*
5 *medicine*, vol. 25, no. 1, pp. 1 – 6, 2002.
- 6 [2] D. A. Low, M. Nystrom, E. Kalinin, P. Parikh, J. F. Dempsey, J. D. Bradley, S. Mutic,
7 S. H. Wahab, T. Islam, G. Christensen, D. G. Politte, and B. R. Whiting, “A method
8 for the reconstruction of four-dimensional synchronized CT scans acquired during free
9 breathing,” *Medical Physics*, vol. 30, no. 6, pp. 1254–1263, 2003.
- 10 [3] T. Pan, “Comparison of helical and cine acquisitions for 4D-CT imaging with multi-
11 slice CT,” *Medical Physics*, vol. 32, no. 2, pp. 627–634, 2005.
- 12 [4] J. M. Reinhardt, K. Ding, K. Cao, G. E. Christensen, E. A. Hoffman, and S. V. Bodas,
13 “Registration-based estimates of local lung tissue expansion compared to xenon CT
14 measures of specific ventilation,” *Medical Image Analysis*, vol. 12, no. 6, pp. 752 –
15 763, 2008, special issue on information processing in medical imaging 2007.
- 16 [5] K. Ding, K. Cao, G. E. Christensen, M. L. Raghavan, E. A. Hoffman, and J. M.
17 Reinhardt, “Registration-based lung tissue mechanics assessment during tidal breath-
18 ing,” in *First International Workshop on Pulmonary Image Analysis*, M. Brown,
19 M. de Bruijne, B. van Ginneken, A. Kiraly, J.-M. Kuhnigk, C. Lorenz, K. Mori, and
20 J. M. Reinhardt, Eds., New York, 2008, p. 63.
- 21 [6] K. Ding, K. Cao, G. E. Christensen, E. A. Hoffman, and J. M. Reinhardt,
22 “Registration-based regional lung mechanical analysis: Retrospectively reconstructed
23 dynamic imaging versus static breath-hold image acquisition,” X. P. Hu and A. V.
24 Clough, Eds., vol. 7262, no. 1. SPIE, 2009, p. 72620D.

- 1 [7] K. Ding, Y. Yin, K. Cao, G. E. Christensen, C.-L. Lin, E. A. Hoffman, and J. M.
2 Reinhardt, "Evaluation of lobar biomechanics during respiration using image reg-
3 istration," in *Proc. of International Conference on Medical Image Computing and*
4 *Computer-Assisted Intervention 2009*, vol. 5761, 2009, pp. 739–746.
- 5 [8] B. P. Yaremko, T. M. Guerrero, J. Noyola-Martinez, R. Guerra, D. G. Lege, L. T.
6 Nguyen, P. A. Balter, J. D. Cox, and R. Komaki, "Reduction of normal lung
7 irradiation in locally advanced non-small-cell lung cancer patients, using ventila-
8 tion images for functional avoidance," *International Journal of Radiation Oncol-*
9 *ogy*Biology*Physics*, vol. 68, no. 2, pp. 562 – 571, 2007.
- 10 [9] T. Yamamoto, S. Kabus, J. von Berg, C. Lorenz, and P. J. Keall, "Impact of four-
11 dimensional computed tomography pulmonary ventilation imaging-based functional
12 avoidance for lung cancer radiotherapy," *Int. J. Radiation Oncology Biol. Phys.*, vol. 2,
13 pp. 1–10, 2010.
- 14 [10] K. Ding, J. E. Bayouth, J. M. Buatti, G. E. Christensen, and J. M. Reinhardt, "4dct-
15 based measurement of changes in pulmonary function following a course of radiation
16 therapy," *Medical Physics*, vol. 37, no. 3, pp. 1261–1272, 2010.
- 17 [11] T. Guerrero, K. Sanders, J. Noyola-Martinez, E. Castillo, Y. Zhang, R. Tapia,
18 R. Guerra, Y. Borghero, and R. Komaki, "Quantification of regional ventila-
19 tion from treatment planning CT," *International Journal of Radiation Oncol-*
20 *ogy*Biology*Physics*, vol. 62, no. 3, pp. 630 – 634, 2005.
- 21 [12] T. Guerrero, K. Sanders, E. Castillo, Y. Zhang, L. Bidaut, and T. P. R. Komaki,
22 "Dynamic ventilation imaging from four-dimensional computed tomography," *Phys*
23 *Med Biol.*, vol. 51, no. 4, pp. 777–791, Feb. 21 2006.
- 24 [13] G. E. Christensen, J. H. Song, W. Lu, I. E. Naqa, and D. A. Low, "Tracking lung
25 tissue motion and expansion/compression with inverse consistent image registration
26 and spirometry." *Med Physics*, vol. 34, no. 6, pp. 2155–2165, June 2007.
- 27 [14] R. Castillo, E. Castillo, J. Martinez, and T. Guerrero, "Ventilation from four-
28 dimensional computed tomography: density versus jacobian methods," *Physics in*
29 *Medicine and Biology*, vol. 55(16), pp. 4661–4685, 2010.
- 30 [15] C. Marcucci, D. Nyhan, and B. A. Simon, "Distribution of pulmonary ventilation
31 using Xe-enhanced computed tomography in prone and supine dogs," *J Appl Physiol*,
32 vol. 90, no. 2, pp. 421–430, 2001.

- 1 [16] J. K. Tajik, D. Chon, C.-H. Won, B. Q. Tran, and E. A. Hoffman, "Subsecond
2 multisection CT of regional pulmonary ventilation," *Academic Radiology*, vol. 9, pp.
3 130–146, 2002.
- 4 [17] D. Chon, B. A. Simon, K. C. Beck, H. Shikata, O. I. Saba, C. Won, and E. A.
5 Hoffman, "Differences in regional wash-in and wash-out time constants for xenon-CT
6 ventilation studies," *Respiratory Physiology & Neurobiology*, vol. 148, no. 1-2, pp. 65
7 – 83, 2005.
- 8 [18] J. Guo, M. K. Fuld, S. K. Alford, J. M. Reinhardt, and E. A. Hoffman, "Pulmonary
9 analysis software suite 9.0: Integrating quantitative measures of function with struc-
10 tural analyses," in *First International Workshop on Pulmonary Image Analysis*, New
11 York, 2008, pp. 283–292.
- 12 [19] K. Cao, K. Ding, G. E. Christensen, and J. M. Reinhardt, "Tissue volume and vessel-
13 ness measure preserving nonrigid registration of lung ct images," B. M. Dawant and
14 D. R. Haynor, Eds., vol. 7623, no. 1. SPIE, 2010, p. 762309.
- 15 [20] K. Cao, K. Ding, G. E. Christensen, M. L. Raghavan, R. E. Amelon, and J. M. Rein-
16 hardt, "Unifying Vascular Information in Intensity-Based Nonrigid Lung CT Regis-
17 tration," in *Biomedical Image Registration*, B. Fischer, B. Dawant, and C. Lorenz,
18 Eds., Lübeck, 2010, pp. 1–12.
- 19 [21] Y. Yin, E. A. Hoffman, and C.-L. Lin, "Local tissue-weight-based nonrigid registration
20 of lung images with application to regional ventilation," X. P. Hu and A. V. Clough,
21 Eds., vol. 7262, no. 1. SPIE, 2009, p. 72620C.
- 22 [22] Y. Yin, E. A. Hoffman, and C.-L. Lin, "Mass preserving nonrigid registration of CT
23 lung images using cubic B-spline," *Medical Physics*, vol. 36, no. 9, pp. 4213–4222,
24 2009.
- 25 [23] K. Cao, G. E. Christensen, K. Ding, and J. M. Reinhardt, "Intensity-and-Landmark-
26 Driven, Inverse Consistent, B-Spline Registration and Analysis for Lung Imagery," in
27 *Second International Workshop on Pulmonary Image Analysis*, M. Brown, M. de Brui-
28 jne, B. van Ginneken, A. Kiraly, J.-M. Kuhnigk, C. Lorenz, J. R. McClelland, K. Mori,
29 A. Reeves, and J. M. Reinhardt, Eds., London, UK, 2009, p. 137.
- 30 [24] Y. Yin, J. Choi, E. A. Hoffman, M. H. Tawhai, and C.-L. Lin, "Simulation of pul-
31 monary air flow with a subject-specific boundary condition," *Journal of Biomechan-
32 ics*, vol. 43, no. 11, pp. 2159 – 2163, 2010.

- 1 [25] E. A. Hoffman and E. L. Ritman, “Effect of body orientation on regional lung expansion in dog and sloth,” *J Appl Physiol*, vol. 59, no. 2, pp. 481–491, 1985.
- 2
- 3 [26] A. F. Frangi, W. J. Niessen, K. L. Vincken, and M. A. Viergever, “Multiscale vessel
4 enhancement filtering,” in *MICCAI*, vol. 1496, 1998, pp. 130–137.
- 5 [27] H. Shikata, E. A. Hoffman, and M. Sonka, “Automated segmentation of pulmonary
6 vascular tree from 3D CT images,” A. A. Amini and A. Manduca, Eds., vol. 5369,
7 no. 1. SPIE, 2004, pp. 107–116.
- 8 [28] H. Shikata, G. McLennan, E. A. Hoffman, and M. Sonka, “Segmentation of pulmonary
9 vascular trees from thoracic 3D CT images,” *International Journal of Biomedical
10 Imaging*, vol. 2009, no. 1, p. 36240.
- 11 [29] V. Joshi, J. M. Reinhardt, and M. D. Abramoff, “Automated measurement of retinal
12 blood vessel tortuosity,” in *Proc. SPIE Conf. Medical Imaging*, N. Karssemeijer and
13 R. M. Summers, Eds., vol. 7624, 2010, p. 76243.
- 14 [30] R. H. Byrd, P. Lu, J. Nocedal, and C. Zhu, “A limited memory algorithm for bound
15 constrained optimization,” *SIAM J. Sci. Comput.*, vol. 16, no. 5, pp. 1190–1208, 1995.
- 16 [31] Y. Choi and S. Lee, “Injectivity conditions of 2D and 3D uniform cubic b-spline
17 functions,” *Graphical Models*, vol. 62, no. 6, pp. 411–427, 2000.
- 18 [32] B. A. Simon, “Non-invasive imaging of regional lung function using X-Ray computed
19 tomography,” *Journal of Clinical Monitoring and Computing*, vol. 16, no. 5, pp. 433
20 – 442, 2000.
- 21 [33] M. K. Fuld, R. B. Easley, O. I. Saba, D. Chon, J. M. Reinhardt, E. A. Hoffman,
22 and B. A. Simon, “CT-measured regional specific volume change reflects regional
23 ventilation in supine sheep,” *J Appl Physiol*, vol. 104, no. 4, pp. 1177–1184, 2008.
- 24 [34] K. Murphy, B. van Ginneken, J. Pluim, S. Klein, and M. Staring, “Semi-automatic
25 reference standard construction for quantitative evaluation of lung CT registration,”
26 in *Proc. of International Conference on Medical Image Computing and Computer-
27 Assisted Intervention 2008*, vol. 5242, 2008, pp. 1006–1013.
- 28 [35] A. Papoulis, Ed., *Probability and Statistics*. Englewood Cliffs, NJ: Prentence Hall,
29 1990.

- 1 [36] S. Kabus, J. von Berg, T. Yamamoto, R. Opfer, and P. J. Keall, “Lung ventilation
2 estimation based on 4D-CT imaging,” in *First International Workshop on Pulmonary*
3 *Image Analysis*, New York, 2008, pp. 73–81.